Dipolar interactions and their influence on the critical single domain grain size of Ni in layered Ni/Al_2O_3 composites

2008 J. Phys.: Condens. Matter 20 385213

(http://iopscience.iop.org/0953-8984/20/38/385213)

IOP PUBLISHING JOURNAL OF PHYSICS: CONDENSED MATTER

J. Phys.: Condens. Matter **20** (2008) 385213 (5pp) doi:10.1088/0953-8984/20/38/385213

Dipolar interactions and their influence on the critical single domain grain size of Ni in layered Ni/Al_2O_3 composites

R Das[1], A Gupta[2], D Kumar[2,3], S H Oh[2,3], S J Pennycook[3] and A F Hebard[1,4]

[1] Department of Physics, University of Florida, Box 118440, Gainesville, FL 32611, USA
[2] Department of Mechanical and Chemical Engineering, North Carolina A&T State University, Greensboro, NC 27411, USA
[3] Materials Science and Technology Division, PO Box 2008, Oak Ridge National Laboratory, Oak Ridge, TN 37831, USA

E-mail: afh@phys.ufl.edu

Received 25 April 2008, in final form 25 July 2008
Published 27 August 2008
Online at stacks.iop.org/JPhysCM/20/385213

Abstract

Pulsed laser deposition has been used to fabricate Ni/Al_2O_3 multilayer composites in which Ni nanoparticles with diameters in the range of 3–60 nm are embedded as layers in an insulating Al_2O_3 host. At fixed temperatures, the coercive fields plotted as a function of particle size show well-defined peaks, which define a critical size that delineates a crossover from coherently rotating single domain to multiple domain behavior. We observe a shift in peak position to higher grain size as temperature increases and describe this shift with theory that takes into account the decreasing influence of dipolar magnetic interactions from thermally induced random orientations of neighboring grains.

(Some figures in this article are in colour only in the electronic version)

1. Introduction

The magnetic properties of nanoparticles have been the focus of many recent experimental and theoretical studies. Technological improvements have now made it possible to reproducibly fabricate nanomagnetic particles with precise particle size and interparticle distances [1–6]. These controlled systems have enabled study of the fundamental properties of single as well as interacting particles. Most applications require that the particles be single domain with a uniform magnetization that remains stable with a sufficiently large anisotropy energy to overcome thermal fluctuations [7], which establishes a temperature-dependent *lower bound* to the particle size. These considerations must take into account the effect of interactions on magnetic properties as is evident for high-density recording media [8] where particles are very close to each other. Considerable insight has already been gained from experimental studies of the effect of dipolar interaction on superparamagnetic relaxation time [9–18] and blocking temperature [18]. Less understood however is the effect of dipolar interactions on the establishment of an *upper bound* to particle size, which defines the crossover from single domain (SD) to multi domain (MD) behavior. In the following we show using coercivity measurements on Ni/Al_2O_3 composites that with increasing temperature this upper bound to particle size increases and then saturates due to attenuated dipolar interactions from thermally induced coherent motions of the magnetization of the neighboring randomly oriented particles.

2. Experimental details

The composite system studied in this paper comprises elongated and polycrystalline Ni particles with diameters in the range of 3–60 nm embedded as layers in an insulating Al_2O_3 host. The multilayer samples were fabricated on Si(100) or sapphire (*c*-axis) substrates using pulsed laser deposition from alumina and nickel targets. High purity targets of Ni (99.99%) and Al_2O_3 (99.99%) were alternately ablated for deposition. Before deposition, the substrates were ultrasonically degreased

[4] Author to whom any correspondence should be addressed.

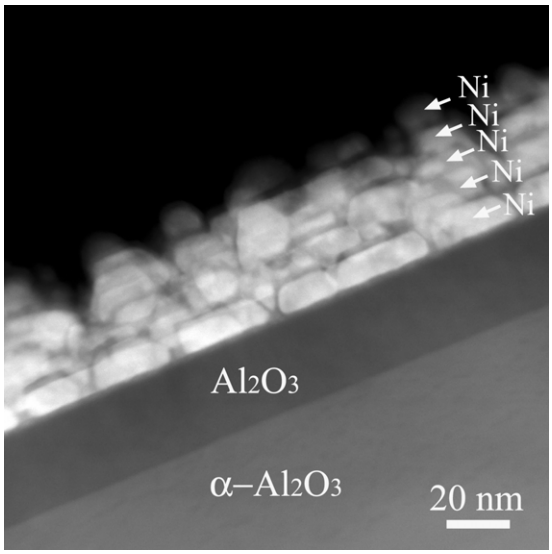

Figure 1. Cross-sectional dark field STEM image of a 5-layer Ni–Al_2O_3 sample grown on *c*-axis sapphire.

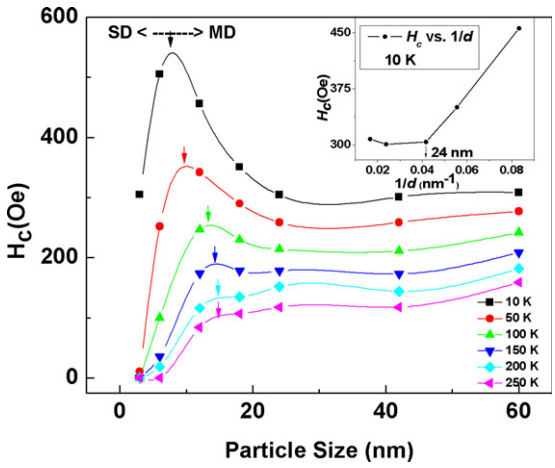

Figure 2. Coercivity for 5-layer Ni/Al_2O_3 multilayer samples (5 repeat units) plotted as a function of particle size (diameter) at the temperatures indicated in the legend. The peak positions at $d = d_c$ for each isotherm, indicated by vertical arrows, delineate the crossover from single domain (SD) behavior ($d < d_c$) to multiple domain (MD) behavior ($d > d_c$). Inset shows the behavior of H_c as a function of $1/d$ for the particles with $d > d_c$ at 10 K. The linear dependence up to 24 nm diameter particles with saturation at a constant value for larger particles [32] is consistent with the behavior expected for multidomain particles. Thus particles on the right-hand side of the peak are multidomain.

and cleaned in acetone and methanol each for 10 min and then etched in a 49% hydrofluoric acid (HF) solution to remove the surface silicon dioxide layer, thus forming hydrogen-terminated surfaces [19]. The base pressure for all the depositions was of the order of 10^{-7} Torr. After substrate heating, the pressure increased to the 10^{-6} Torr range. The substrate temperature was kept at about 550 °C during growth of the Al_2O_3 and Ni layers. The repetition rate of the laser beam was 10 Hz and energy density used was $\sim$2 J cm^{-2} over a spot size 4 mm $\times$ 1.5 mm. A 40 nm-thick buffer layer of Al_2O_3 was deposited initially on the Si or sapphire substrate before the sequential growth of Ni and Al_2O_3. This procedure results in a very smooth starting surface for growth of Ni as verified by high resolution scanning transmission electron microscopy (STEM) studies (figure 1). Multilayer samples were prepared having 5 layers of Ni nanoparticles spaced from each other by 3 nm-thick Al_2O_3 layers. A 3 nm-thick cap layer of Al_2O_3 was deposited to protect the topmost layer of Ni nanoparticles.

Shown in figure 1 is a cross-sectional STEM image from a multi-layered (5 layers) Ni-Al_2O_3 sample grown on *c*-plane sapphire. The Ni particles have a size of 23 $\pm$ 5 nm in width and $\sim$9 nm in height. The separation between neighboring particles is on the order of 3 nm (measured as a projected distance in cross-sectional view), which is comparable to the thickness of the Al_2O_3 spacer layers. For the purposes of this experiment the 'grain size' d, as measured by the amount of Ni deposited referenced to a calibrated standard, represents the average size of the disk-shaped grains shown in the figure. This 'calibration' was obtained from cross-sectional TEM micrographs of single layer samples [20] by comparing the average grain size with d. The STEM observation also shows that the Al_2O_3 spacer layers are partially crystallized. Due to the large surface energy difference between Ni and Al_2O_3, Ni forms well-defined, separated islands within the Al_2O_3 matrix [20]. Previous studies on similarly-prepared samples using atomic number (Z) contrast imaging in STEM together with electron energy loss spectroscopy (EELS) have confirmed the absence of NiO at the Ni/Al_2O_3 interfaces [20]. The Ni/Al_2O_3 interfaces were chemically abrupt without an intermixing between Ni, Al and oxygen. In addition we did not observe exchange-bias induced asymmetric magnetization loops, thus lending support to the conclusions of previous studies [20] that antiferromagnetic NiO is absent in our layered Ni/Al_2O_3 system.

Previous STEM studies on single layer samples have shown the particles to be polycrystalline with, for example, a three nm particle comprising three crystalline grains [20]. Polycrystalline particles will therefore have crystalline grains oriented in different directions, thus tending to average any net crystalline anisotropy to zero. Accordingly, temperature-independent shape anisotropy is dominant and temperature-dependent crystalline anisotropy can be neglected. In addition, it is also important to note that the exchange length l_{ex} = 14.6 nm for Ni, [21] which is the length scale below which atomic exchange interactions dominate over magnetostatic fields, determines the critical radii (R_{coh}) for coherent rotation: $R_{coh} \cong 5l_{ex}$ for spherical particles and $R_{coh} \cong 3.5l_{ex}$ for nanowires [22]. The particle sizes (1.5–30 nm in radius) that we have investigated are thus smaller than the critical radius below which coherent rotation of Ni prevails.

In figure 2 we show plots of H_c as a function of particle size d at each of the temperatures indicated in the legend. Coercive fields were extracted from magnetization loops measured by a Quantum Design superconducting quantum interference device (SQUID) after subtracting out the diamagnetic contribution from the substrate. Magnetic field was applied along the plane of the films. To obtain the magnetization loops, the magnetic field was varied over the

full range (±5 T) while keeping temperature fixed. The high magnetic field data show linear magnetization with magnetic field, which is due to the diamagnetic contribution from the substrate (as signal from ferromagnetic Ni particles saturates at high magnetic fields) and can thus be subtracted from the data. The decrease of H_c with increasing temperature for fixed d is clearly apparent and can be understood as the effect of thermal fluctuations [23]. For the low-temperature isotherms, there are pronounced peaks which define a temperature-dependent critical particle size d_c delineating SD ($d < d_c$) behavior of *coherently rotating particles* from MD ($d > d_c$) behavior [23–31]. In the inset of figure 2 we have plotted H_c versus $1/d$ for the particles of size $d > d_c$ at 10 K. It is clear that H_c behave linearly with $1/d$ up to particle size of 24 nm and then saturates. This behavior is consistent with the dependence expected for multidomain particles [32] Thus particles of size $d > d_c$ are multidomain and the peak defines the crossover from SD to MD behavior. The formation of domain structure is driven by the reduction of long range magnetostatic energy, which at equilibrium is balanced by shorter range exchange and anisotropy energy costs associated with the spin orientations within a domain wall. The purpose of this paper is to show that this well-defined SD region of coherently rotating particles extends over a larger range of grain sizes at higher temperatures because of the diminishing influence of dipolar interactions from neighboring grains.

3. Data and discussion

The influence of dipolar interactions on the SD/MD crossover can be understood in a qualitative way by considering the three randomly oriented particles shown schematically in the inset of figure 3. Particle 1 experiences dipolar fields from particles 2 and 3, which are not colinear for most orientations for a randomly oriented particle system. Because dipolar fields decrease rapidly with interparticle separation, the dipolar field due to particle 3 (2) will be stronger than particle 2 (3) on the left (right) side of the particle 1. The separate and unequal influence of the neighboring particles thus favors the formation of domains in particle 1.

To make these notions more quantitative, we modify the treatment of Dormann *et al* [10] for interacting paramagnets to include the temperature region below the blocking temperature T_B and find the temperature-dependent dipolar magnetic field H_d arising from temperature induced fluctuations in the magnetization of nearest neighbor nanometer size particles to be,

$$H_d = \frac{\mu_0 M_s a}{4\pi} \frac{e^{\beta}(1-e^{-1})}{\sqrt{\pi\beta}\left(\mathrm{erfi}(\beta) - \mathrm{erfi}(\sqrt{\beta-1})\right)} \xrightarrow[T\to 0]{} \frac{\mu_0 M_s a}{4\pi}, \quad (1)$$

where erfi is the imaginary error function, M_s is the saturation magnetization, $\beta = KV/k_BT$, and $a = V(3\cos^2\xi - 1)/s^3$ is a dimensionless parameter with ξ and s corresponding respectively to an angle parameter and the separation between two adjacent particles each with volume V. The parameter β is always greater than one for $T < T_B$ where there is still coercivity; i.e., the magnetization is fluctuating but not going over barriers.

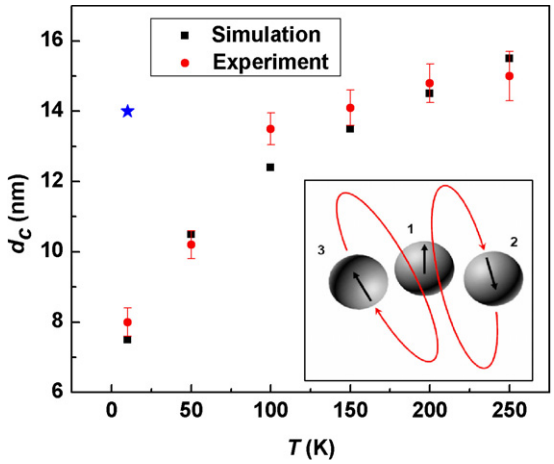

Figure 3. Peak position, d_c, plotted as a function of temperature (red circles). The black squares are the results derived from equation (4). The blue star represents the observed value of d_c for a series of single layer samples at 10 K. The inset, a schematic of three neighboring particles oriented in different directions, illustrates how the dipolar fields from particles 2 and 3 facilitate the formation of domains in particle 1, as the dipolar magnetic fields are in different directions.

The derivation of equation (1) includes averaging over the accessible directions of magnetization weighted by a Boltzmann factor. Higher temperatures give smaller magnetizations since the particles fluctuate over larger angles. Specifically, spin up and down particles will be in energy minima separated by an anisotropy energy barrier. At absolute zero temperature only the direction corresponding to the minima of the energy will be occupied. At finite temperatures, according to the Boltzmann law, other energy states will be occupied around this minimum and will have different directions of magnetizations. Thus to obtain the actual magnetization, an average over all these accessible directions is calculated, constrained by the fact that the probability of those states to be occupied is given by Boltzmann factor

$$\langle M\rangle_T = M_s \frac{\int_{\theta\,\min}^{\theta_T} \exp[-\frac{E(\theta)}{k_BT}]\cos\theta\,\mathrm{d}\theta}{\int_{\theta\,\min}^{\theta_T} \exp[-\frac{E(\theta)}{k_BT}]\mathrm{d}\theta}, \quad (2)$$

where at zero magnetic field $E(\theta) = KV\sin^2\theta$. Thus $\theta_{\min} = 0$ and θ_T is temperature dependent, obeying the relation, $\sin^2\theta_T = k_BT/KV$. The parameter θ_T will be higher at higher temperatures and thus the thermal average of the magnetization will diminish at higher temperatures. Using equation (2) one can determine the temperature dependence of the dipolar magnetic field H_d as shown in equation (1) for particles treated as simple dipoles.

In the absence of interactions ($H_d = 0$) the condition for the SD to MD transition is given for spherical particles with radius $d/2$ by, $Ad_c^3 = Bd_c^2$, where Ad_c^3 is the total magnetostatic energy and $E_{dw} = Bd_c^2$ is the domain wall energy [33]. We have absorbed the factor of two, which relates diameter to radius, into the constants A and B. In the presence

of the dipolar magnetic field H_d, the formation of domain walls will be assisted by a Zeeman term which is proportional to the volume of the affected particle. The condition determining the SD to MD transition now becomes,

$$Ad_c^3 = Bd_c^2 - \pi M_s H_d d_c^3/6. \quad (3)$$

When the dipolar interaction is a small perturbation, i.e., $M_s H_d/A \ll 1$, equations (1) and (3) can be combined to give the relation,

$$d_c = d_{c0} - d_{dw}\frac{e^{\beta}(1-e^{-1})}{\sqrt{\pi\beta}\left(\mathrm{erfi}(\beta) - \mathrm{erfi}(\sqrt{\beta-1})\right)}, \quad (4)$$

where $d_{c0} = B/A$ is the temperature-independent critical diameter in the absence of interactions (high-temperature limit) and $d_{dw} = \mu_0 B M_s^2 \pi/(72A^2)$ for $a = \pi/3$. The second term on the right-hand side of equation (4) thus becomes a temperature-dependent correction to d_c due to interactions from neighboring particles and decreases with increasing T.

Since the dipole–dipole interactions are weaker at higher temperatures (equation (1)), the nanoparticles remain in the SD state to a larger size, which by equation (4) results in a shift of d_c towards higher values at higher temperatures. This is indeed evident in figure 3, which shows the temperature dependence of d_c as determined from the data in figure 2. The black squares are the simulated data according to equation (4) using the two fitting parameters: d_{c0} and d_{dw}. Qualitatively, the data agree quite well with the prediction of the theoretical model without taking into account the topology and size distribution of the particles. We have found $d_{c0} = 84$ nm from our simulation (figure 3, black squares) to be close to the value for a particle with shape anisotropy constant $K_{shape} = 3.1 \times 10^4$ J m^{-3} ($d_{c0} = 72\sqrt{A_{ex}K}/\mu_0 M_s^2$, where A_{ex} is exchange stiffness, K is anisotropy constant) [22]. Values of A ($\propto \mu_0 M_s^2$) and B ($\propto \sqrt{A_{ex}K}$) have been found to be 1.44×10^4 J m^{-3} and 1.21×10^{-3} J m^{-2} respectively. This value of A is very close to the theoretical predicted value [22] and the value of B is again consistent with the value of the shape anisotropy. The value of the shape anisotropy can also be predicted from the zero-temperature extrapolation $H_{co} \sim K/M_s$ for randomly oriented particles [22]. For $K_{shape} = 3.1 \times 10^4$ J m^{-3}, $H_{co} \sim 620$ Oe. This is in good agreement with the 500 Oe coercive field observed at 10 K for the 6 nm sample.

For a separate series of single layer samples the coercivities at 10 K peak at $d_c = 14$ nm as shown in figure 3 by the blue star. In the single layer samples the peak position occurs at higher particle size (14 nm) than multilayer samples (8 nm). This difference reinforces our interpretation and can be understood by realizing that the dipolar interactions of the single layer samples are significantly reduced compared to the multilayer samples because of the smaller number of nearest neighbors.

4. Conclusion

In summary, we have fabricated magnetic nanoparticles in an insulating thin film matrix with tunable properties achieved by varying particle size and temperature. The peaks in the coercivity isotherms delineate a critical grain size d_c which identifies the crossover from SD to MD behavior. The presence of dipolar interactions and their diminishing influence with increasing temperature is responsible for the observed dependence of d_c on temperature and is in good qualitative agreement with our modification of present theory [10] of interacting particles. The well-established influence of dipolar interactions on superparamagnetic relaxation time [9–18] together with the connection between relaxation time τ and coercivity H_c suggests that there is a concomitant influence of dipolar interactions on the coercivity observed near the superparamagnetic limit where $H_c = 0$. The work reported here extends this connection to the upper limits on the size of SD particles by showing that dipolar interactions can facilitate the formation of multi domain particles especially at low temperatures.

Acknowledgments

This research was performed as a part of the Nanoscale Interdisciplinary Research Team project supported by the US National Science Foundation grant number DMR-0403480. We thank R Skomski for useful discussions and comments.

References

[1] Mamiya H, Nakatani I and Furubayashi T 2000 Phase transitions of iron-nitride magnetic fluids *Phys. Rev. Lett.* **84** 6106–9
[2] Jamet M *et al* 2001 Magnetic anisotropy of a single cobalt nanocluster *Phys. Rev. Lett.* **86** 4676–9
[3] Stamm C *et al* 1998 Two-dimensional magnetic particles *Science* **282** 449–51
[4] Sun S H, Murray C B, Weller D, Folks L and Moser A 2000 Monodisperse FePt nanoparticles and ferromagnetic FePt nanocrystal superlattices *Science* **287** 1989–92
[5] Puntes V F, Krishnan K M and Alivisatos A P 2001 Colloidal nanocrystal shape and size control: the case of cobalt *Science* **291** 2115–7
[6] Babonneau D, Petroff F, Maurice J L, Fettar F, Vaures A and Naudon A 2000 Evidence for a self-organized growth in granular Co/Al_2O_3 multilayers *Appl. Phys. Lett.* **76** 2892–4
[7] Skumryev V, Stoyanov S, Zhang Y, Hadjipanayis G, Givord D and Nogues J 2003 Beating the superparamagnetic limit with exchange bias *Nature* **423** 850–3
[8] Sellmyer D J, Yu M and Kirby R D 1999 Nanostructured magnetic films for extremely high density recording *Nanostruct. Mater.* **12** 1021–6
[9] Dormann J L *et al* 1996 Thermal variation of the relaxation time of the magnetic moment of gamma-Fe_2O_3 nanoparticles with interparticle interactions of various strengths *Phys. Rev.* B **53** 14291–7
[10] Dormann J L, Bessais L and Fiorani D 1988 A dynamic study of small interacting particles—superparamagnetic model and spin-glass laws *J. Phys. C: Solid State Phys.* **21** 2015–34
[11] Luo W L, Nagel S R, Rosenbaum T F and Rosensweig R E 1991 Dipole interactions with random anisotropy in a frozen ferrofluid *Phys. Rev. Lett.* **67** 2721–4
[12] Mørup S and Tronc E 1994 Superparamagnetic relaxation of weakly interacting particles *Phys. Rev. Lett.* **72** 3278–81
[13] Mørup S, Bodker F, Hendriksen P V and Linderoth S 1995 Spin-glass-like ordering of the magnetic-moments of interacting nanosized maghemite particles *Phys. Rev.* B **52** 287–94

[14] Hansen M F and Mørup S 1998 Models for the dynamics of interacting magnetic nanoparticles *J. Magn. Magn. Mater.* **184** 262–74
[15] Jonsson P E and Garcia-Palacios J L 2001 Relaxation time of weakly interacting superparamagnets *Europhys. Lett.* **55** 418–24
[16] Elhilo M, Ogrady K and Chantrell R W 1992 Susceptibility phenomena in a fine particle system. 1. concentration-dependence of the peak *J. Magn. Magn. Mater.* **114** 295–306
[17] Andersson J O, Djurberg C, Jonsson T, Svedlindh P and Nordblad P 1997 Monte Carlo studies of the dynamics of an interacting monodispersive magnetic-particle system *Phys. Rev.* B **56** 13983–8
[18] Garcia-Otero J, Porto M, Rivas J and Bunde A 2000 Influence of dipolar interaction on magnetic properties of ultrafine ferromagnetic particles *Phys. Rev. Lett.* **84** 167–70
[19] Kern W and Puotinen D A 1970 Cleaning solutions based on hydrogen peroxide for use in silicon semiconductor technology *RCA Rev.* **31** 187
[20] Kumar D, Pennycook S J, Lupini A, Duscher G, Tiwari A and Narayan J 2002 Synthesis and atomic-level characterization of Ni nanoparticles in Al_2O_3 matrix *Appl. Phys. Lett.* **81** 4204–6
[21] Kong L S and Chou S Y 1996 Effects of bar length on switching field of nanoscale nickel and cobalt bars fabricated using lithography *J. Appl. Phys.* **80** 5205–8
[22] Skomski R 2003 Nanomagnetics *J. Phys.: Condens. Matter* **15** R841–96
[23] Cullity B D 1972 *Introduction to Magnetic Materials* (Reading, MA: Addison-Wesley) p 1972
[24] Kneller E F and Luborsky F E 1963 Particle size dependence of coercivity and remanence of single-domain particles *J. Appl. Phys.* **34** 656
[25] Tenzer R K 1963 Influence of particle size on coercive force of barium ferrite powders *J. Appl. Phys.* **34** 1267–9
[26] Sanchez R D, Rivas J, Vaqueiro P, Lopez-Quintela M A and Caeiro D 2002 Particle size effects on magnetic garnets prepared by a properties of yttrium iron sol–gel method *J. Magn. Magn. Mater.* **247** 92–8
[27] Luna C, Morales M D, Serna C J and Vazquez M 2003 Multidomain to single-domain transition for uniform $Co_{80}Ni_{20}$ nanoparticles *Nanotechnology* **14** 268–72
[28] Zhang T, Li G, Qian T, Qu J F, Xiang X Q and Li X G 2006 Effect of particle size on the structure and magnetic properties of $La_{0.6}Pb_{0.4}MnO_3$ nanoparticles *J. Appl. Phys.* **100** 094324
[29] George M, Nair S S, John A M, Joy P A and Anantharaman M R 2006 Structural, magnetic and electrical properties of the sol–gel prepared $Li_{0.5}Fe_{2.5}O_4$ fine particles *J. Phys. D: Appl. Phys.* **39** 900–10
[30] Jiang J and Yang Y M 2007 Facile synthesis of nanocrystalline spinel $NiFe_2O_4$ via a novel soft chemistry route *Mater. Lett.* **61** 4276–9
[31] Rojas D P, Barquin L F, Fernandez J R, Espeso J I and Sal J C G 2007 Size effects in the magnetic behaviour of $TbAl_2$ milled alloys *J. Phys.: Condens. Matter* **19** 186214
[32] Rowlands G 1976 Variation of coercivity with particle-size *J. Phys. D: Appl. Phys.* **9** 1267–9
[33] Kittel C 1949 Physical theory of ferromagnetic domains *Rev. Mod. Phys.* **21** 541–83